IN-44
90706
43P.

DOE/NASA/3277-4
NASA CR-180812

Performance and Aerodynamic Braking of a Horizontal-Axis Wind Turbine from Small-Scale Wind Tunnel Tests

H.V. Cao and W.H. Wentz, Jr.
Wichita State University

July 1987

Prepared for
NATIONAL AERONAUTICS AND SPACE ADMINISTRATION
Lewis Research Center
Under Grant NSG-3277

for
U.S. DEPARTMENT OF ENERGY
Conservation and Renewable Energy
Wind/Ocean Technology Division

DISCLAIMER

Printed in the United States of America

Available from
National Technical Information Service
U.S. Department of Commerce
5285 Port Royal Road
Springfield, VA 22161

NTIS price codes[1]
Printed copy: A03
Microfiche copy: A01

[1]Codes are used for pricing all publications. The code is determined by the number of pages in the publication. Information pertaining to the pricing codes can be found in the current issues of the following publications, which are generally available in most libraries: *Energy Research Abstracts (ERA); Government Reports Announcements* and Index (*GRA* and I); *Scientific and Technical Abstract Reports (STAR);* and publication, NTIS-PR-360 available from NTIS at the above address.

DOE/NASA/3277-4
NASA CR-180812

Performance and Aerodynamic Braking of a Horizontal-Axis Wind Turbine from Small-Scale Wind Tunnel Tests

H.V. Cao and W.H. Wentz, Jr.
Wichita State University
Wichita Falls, Kansas 67208

July 1987

Prepared for
National Aeronautics and Space Administration
Lewis Research Center
Cleveland, Ohio 44135
Under Grant NSG-3277

for
U.S. DEPARTMENT OF ENERGY
Conservation and Renewable Energy
Wind/Ocean Technology Division
Washington, D.C. 20545
Under Interagency Agreement DE-AI01-76ET20320

INTRODUCTION

One of the most critical design requirements for large scale horizontal-axis wind turbines is to provide cost-effective, reliable methods for overspeed control. Overspeed protection is definitely needed when there is a sudden loss of electrical load or in very high wind conditions.

At the present time, large scale horizontal-axis wind turbines utilize partial or full span variable blade pitch to regulate rotor speed. In order to pitch either the full length or a portion of a large wind turbine blade, large blade pitch bearing assemblies and linkages are needed. The design of these systems poses several difficult structural and mechanical problems and adds considerably to system weight and cost (ref. 1).

Alternate methods which require much smaller bearings and pitch actuator systems, and therefore appear to have potential for reducing rotor costs, are the use of spoilers or ailerons as aerodynamic control devices. Spoilers or ailerons, when deflected, change the lift and drag characteristics of the basic airfoil, producing corresponding changes in rotor torque.

Prior to the present project, spoilers of different sizes and deflection angles were tested on an NACA 23024 airfoil 2-D model (ref. 2). Due to promising results, these spoilers were later tested on a twenty-inch diameter rotor (ref. 3). The results of these tests show that the 20 percent chord spoiler at 90 degrees angle of deflection and with hingeline position located at 10 percent chordline on the upper surface of the airfoil produced negative torque for all tip-speed ratios greater than or equal to 0.78. However, since the blade structure is typically located primarily in the forward 50 percent of the airfoil section, it is difficult to design a spoiler system for this hingeline position without a

significant reduction in strength, or alternatively, a substational increase in weight.

Ailerons have also been evaluated as aerodynamic control devices. The primary reason for the preference of ailerons over spoilers is that the entire moveable surface is located on the aft 50 percent of the airfoil making it possible to carry the main rotor structure (main spar) uninterrupted from hub to tip. This simplifies and lightens the structure. Furthermore, ailerons, unlike spoilers, have the capability of providing both positive and negative increments in lift. The lift coefficient can be increased by deflecting the aileron upward. Upward aileron deflection will cause the lift to decrease which, in turn, reduces torque. Studies of predicted rotor performance based on wind tunnel tests of ailerons on a 3-D reflection plane model (ref. 4) indicates a strong possibility of slowing the rotor down to a very low tip-speed ratio. The purpose of the present project is to evaluate the performance of the vented aileron/ deflector combination in a test which includes 3-D induced effects and possible spanwise boundary layer effects.

Earlier studies (ref. 4) have shown that a plain (unvented) aileron with or without lower surface deflector was adequate for power modulation, but inadequate for full aerodynamic braking. These studies also revealed discrepancies between analysis of rotor performance from 2-D wind tunnel data and actual rotor performance. The conclusions from the earlier research are as follows: (1) Aileron control is structurally and mechanically feasible; (2) the ailerons tested were adequate for power modulation, but marginal for aerodynamic braking; nd (3) rotor analysis codes are questionable for predicting effectiveness of aerodynamic braking devices, at least for one case. Thus, even though airfoil section tests and analysis indicate that the vented aileron deflector is adequate, rotating tests are essential for verification. Small scale wind tunnel tests have Reynolds number and model detail limitations, yet they are relatively low-cost, quick, and provide data of high quality in a

controlled environment. It is on this basis that the present tests were planned.

For this project a twenty-inch diameter untapered, untwisted, and unpitched rotor equipped with an aileron over the outboard 30 percent span was tested. The hingeline position was designed such that an upward aileron deflection opens a gap between the aileron and the airfoil. Aileron chord was 30 percent, and a lower 20 percent chord solid extension plate was used to extend the lower surface of the aileron. This configuration was developed in airfoil wind tunnel tests conducted earlier (ref. 4). The purpose of the special hingeline position and the extension plate is to force air to flow upward through the gap at high angles of attack. This upward flow causes the lift to decrease, thus reducing chordwise suction force.

Performance characteristics of an NACA 23024 rotor and an NACA 64_3-621 rotor without ailerons were also studied both experimentally and analytically. Analytical results were obtained by using the wind turbine performance computer program WIND-II (ref. 5). One purpose of the present studies is to correlate rotor performance prediction from 2-D data with rotating experiments.

Surface flow patterns were studied using fluorescent mini-tufts attached to the suction side of the rotor. The purpose of the flow study was to determine the extent and nature of spanwise flow along the rotor at high angles of attack.

This report is an extension of a master of science thesis by the first author (ref. 6). The report includes transition strip results and additional analytical calculations from WIND-II not reported earlier.

LIST OF SYMBOLS

a	Wind retardation (induction) factor
A	Area swept by rotor disk, ft^2
c	Blade chord, ft
C_D	Coefficient of drag
C_L	Coefficient of lift
C_N	Coefficient of normal force
C_S	Coefficient of suction
C_P	Coefficient of power, $P/(qAV_W)$
C_T	Coefficient of thrust, $T/(qA)$
g	Gravitational acceleration, 32.2 ft/sec^2
M	Freestream Mach number
M_t	Tip Mach number
P	Power, W
q	Tunnel dynamic pressure, psf
Q	Torque, lb-ft
r	Radial location along blade, in
R	Blade tip radius, in
Re_W	Freestream Reynolds number per unit length, $\rho V_W/u$
Re_t	Tip chord Reynolds number, $RE_W(c)(1 + TSR^2)^{1/2}$
rpm	Rotational speed in revolutions per minute
T	Thrust, lb
TS	Transition Strips, each 0.005" thick x 0.10" wide
TSR	Tip-speed ratio, V_T/V_W
V_R	Resultant velocity, ft/s
V_T	Blade tip velocity, ΩR, ft/s
V_W	Freestream wind velocity, ft/s
α	Angle of attack, deg
δ_a	Angle of aileron deflection (negative upward), deg
μ	Coefficient of dynamic viscosity, lb_f-sec/ft^2
ρ	Air density, slugs/ft^3
Ω	Angular velocity, rad/s

BACKGROUND

The performance of a horizontal axis wind turbine can be analyzed from the action of the aerodynamic forces on the turbine blade. The blade is analyzed using chordwise strips along the span so that the two-dimensional analysis can be used on each element. Overall blade forces and moments are obtained by summing element contributions. Figure 1 shows a system of forces acting on a wind turbine blade element. The combination of the wind velocity, V_W, the induction factor, a, and the element's velocity caused by blade rotation, Ωr, forms an effective or a resultant wind velocity, V_R. This resultant wind velocity causes lift and drag forces on the blade element. Many large scale wind turbines utilize blades with zero pitch and zero twist. For these blades, the torque, Q (positive in the direction of rotation) is produced only by the force component in the direction parallel to the airfoil chordline, while the thrust, T, (positive in the downstream direction) is produced only by the force component in the direction normal to the airfoil chordline. In nondimensional forms, the torque-producing component is called chordwise suction coefficient, C_S, and the thrust-producing component is called normal coefficient C_N. The component C_S is taken positive in the direction toward the leading edge of the airfoil so that positive C_S produces positive power. The component C_N is defined positive in the positive thrust (downwind) direction. The mathematical relationships between these components and lift and drag coefficients are:

$$C_S = C_L \sin(\alpha) - C_D \cos(\alpha) \qquad (1)$$

$$C_N = C_L \cos(\alpha) + C_D \sin(\alpha) \qquad (2)$$

where C_L is the traditional airfoil sectional lift coefficient and C_D is the traditional sectional drag coefficient. The effective angle of attack, α, is formed by the resultant wind velocity and the airfoil chordline (which is in the plane of rotation for the case of a zero-twist

and zero-pitch wind turbine blade). Since the local tangential velocity decreases with decreasing radius along the span, the angle of attack is higher for inboard blade stations. Figure 2 shows the effects of tip-speed ratio and local blade radius on the local angle of attack. For a normal operating tip-speed ratio of about 5, the angles of attack range from approximately 12 to 20 degrees for the outer 50 percent portion of the blade.

The purpose of the present project is to reduce the rotational speed of the wind turbine under no-load conditions. Studies have shown that for tip-speed ratios of about 7.0 or less, a small mechanical brake could be utilized to bring the rotor to a complete stop. At this tip-speed ratio, the range of angles of attack is from 60 to 90 degrees for all stations along the blade span. Therefore, studies of airfoil characteristics at very high angles of attack are essential for slow-down analysis of wind turbines.

FACILITY AND INSTRUMENTATION

All tests were conducted in the 7 x 10 foot Walter Beech Memorial Wind Tunnel at Wichita State University, with the test assembly installed as shown in figure 3. Instrumentation consisted of a special force-moment balance in which a 10 hp variable-speed, water-cooled, variable-frequency model motor was mounted. This force balance is fitted with strain-gaged flexures so that torque and thrust can be measured directly. The motor speed can be controlled by means of a variable frequency external excitation system. Rotor speed was measured by a signal generator mounted internally. Force data acquisition and processing were accomplished by a Hewlett-Packard Model 21MX mini-computer located in the tunnel control room. These force data were corrected using wind tunnel corrections for solid blockage and wake blockage as given in reference 7. The ratio of rotor disk area to tunnel cross-section area is only 0.0321, making solid and wake blockage corrections small. Traditional wind turbine performance

parameters were calculated using a data reduction computer program available in the WSU Walter Beech Wind Tunnel. These quantities were then recorded, tabulated and plotted.

Surface flow patterns were observed using fluorescent mini-tufts attached to the suction (downwind) side of the rotor-blade, with illumination provided by a 400 watt-second studio strobe light with a UV-passing filter (Corning Glass no. 5970). Flow patterns were then photographed by a motorized, remote-control Pentax LX camera fitted with a 200 mm lens and a Wratten 2B filter; the camera was fixed to a special tripod located about 10 rotor diameters downstream.

MODEL DESCRIPTION

Figure 4 shows the geometry of the rotor models. Three rotor models were used in these tests. All three rotors have the planform shown in figure 4(a), with diameters of 20 inches and chords of 1.75 inches. These models have airfoil sections for all stations from 21 percent span to the tip. The hub sections are rectangular with rounded edges out to 10 percent span, with a tapered transition to the airfoil section at 21 percent span. The solidity factor (blade planform area/swept disk area) of these rotors is 0.111.

The first model uses the NACA 23024 airfoil (fig. 4(b)) and the second model uses the NACA 64_3-621 airfoil (fig. 4(c)) for stations from 21 percent to the tip. The third model utilizes the NACA 23024 airfoil, modified to incorporate a 30 percent chord aileron at -90 degree fixed deflection from 70 percent span to the tip. The geometry of this aileron section is shown in figure 4(d). The hingeline position of the aileron is at 80 percent along the chord from the leading edge and 14 percent above the airfoil chordline. An extension plate or deflector is attached to the high pressure side of the aileron extending forward for a distance equal to 20 percent of the airfoil chord. Coordinates for the NACA 23024 airfoil

and the NACA 64_3-621 airfoil (ref. 8) are given in the Appendix.

The aileron/deflector geometry and hingeline location were determined from airfoil section tests documented in reference 4. The vented deflector aileron presented a special challenge for model fabrication because of the high centrifugal loading (7000 g's) associated with operation at 5000 rpm. The aileron was fabricated from solid maple (the section removed by cutting from the basic planform). The deflector was fabricated from a graphite composite laminate, and the aileron/deflector assembly was attached to the rotor by a series of graphite fibers looped to form a tension "belt" which was bonded into the main blade to carry the centrifugal forces.

RESULTS AND DISCUSSION

For most tests reported here, rotor speed was kept constant and tunnel dynamic pressure was varied. The rotor speeds ranged from 600 to 5,500 rpm and the tunnel dynamic pressure was varied from 1 to as much as 50 psf. The purpose of testing at high tunnel dynamic pressure and low rpm was to obtain very low tip-speed ratios. Test tip-speed Reynolds numbers and tip-speed Mach numbers are given in Table 1. Results are presented in terms of thrust and power coefficients as a function of tip-speed ratio (TSR), and rotor power output as a function of wind speed.

Analytical studies were conducted for most of the configurations tested using WIND-II, a FORTRAN code for predicting rotor performance (ref. 5). One of the input requirements for WIND-II is a set of 2-D lift and drag coefficient data as functions of angle of attack for the airfoil section on the rotor. It is important to note that all 2-D data used as inputs to WIND-II were from tests of a 9-inch chord, 36-inch span model which were obtained at the Reynolds number of 0.6×10^6 (refs. 2 and 9). Chord Reynolds numbers for the present tests were lower, ranging from 0.02×10^6 at the inboard station to 0.11×10^6 at the tip, for low

rpm tests. For the highest rpm tests, the chord Reynolds numbers ranged from 0.11×10^6 at the inboard station to 0.58×10^6 at the tip.

Tests of the Clean NACA 23024 Rotor Without Ailerons

Figures 5 and 6 present the results of testing the NACA 23024 rotor without the ailerons and without transition strips (clean). Since the aerodynamic characteristics of airfoils at low Reynolds numbers are often dominated by laminar separation, transition location effects were studied analytically using 2-D data with 1, 2 and 3 transition strips (from ref. 4) as inputs to WIND-II. Results of these studies are compared to experimental measurements as shown in Figure 5.

Figure 5 shows a plot of thrust coefficient as a function of TSR for the clean NACA 23024 rotor. As predicted by WIND-II, the thrust coefficient of this rotor increases with TSR. Theoretical calculations show that the case with no transition strip shows the best agreement with the experimental measurements, although all cases show about the same trend.

The effects of transition strips are much more significant on power coefficient than thrust coefficient. Figure 5(b) shows a plot of power coefficient as a function of tip-speed ratio. Experimental data shows that the rotor state of zero-power occurred at the TSRs of 1.5, 4.0 and 8.0. Maximum power coefficient occurred at TSR of about 5.0. Theoretical calculations with no transition strip show a somewhat higher C_p peak than experimental results. Transition strips reduce maximum predicted C_p. The analysis based on 2-D data with one transition strip produces about the same maximum power coefficient as the clean rotor tests.

Power calculated and plotted as a function of wind speed is shown in figures 6(a) through (c) for rotor speeds of 2000, 3000 and 4000 rpm, respectively. For all three cases, theoretical calculations from WIND-II

over-predicted the peak power and the cut-out wind speed for the rotor. The analysis, however, agrees very well with the experimental measurements for the portion of the power curve from the point of cut-in velocity to the point where experimental data shows maximum power is reached (blade section stalling).

One reason WIND-II predictions may differ from the rotor experiments is that the airfoil section data used as a input to WIND-II were from tests at a Reynolds number of 0.6×10^6, while rotor Reynolds numbers were substantially lower. It is recommended, therefore, that tests be conducted to obtain low Reynolds number airfoil data for these blade sections. The lower Reynolds number airfoil section data should then be used as inputs to WIND-II to refine the predicted performance of the rotor blade. The Mach number differences between non-rotating and rotating experiments are not considered significant.

Tests of the Clean NACA 64_3-621 Rotor

The test results of the NACA 64_3-621 rotor without transition strips are presented in terms of nondimensional parameters as shown in figure 7 and rotor power output as shown in figure 8.

As shown in figure 7(a), theoretical calculations are similar to experimental measurements for thrust coefficient as a function of TSR. In figure 7(b) the tests show a somewhat higher maximum power coefficient, but in general the agreement is very good. A very interesting point for these tests is that the NACA 64_3-621 rotor had only one speed (TSR of 6.7) for which power is zero, while the theoretical calculations from WIND-II predict states of zero-power for the rotor to occur at TSRs of 0.4, 2.0 and 6.7.

Figure 8 presents the results for the NACA 64_3-621 rotor in terms of power as a function of wind speed. Similar to the results for the NACA

23024 rotor, analytical calculations over-predict the peak-power, and agree with experimental measurements only from the point of cut-in velocity to the point of maximum power measured experimentally. As wind velocity is increased, however, results from this series of tests are no longer similar to those of the NACA 23024 rotor. Furthermore, calculations from WIND-II fail to predict the cut-out wind speed of the NACA 64_3-621 rotor. Figure 8(a) shows the plot of power as a function of wind speed for the NACA 64_3-621 rotor at 2000 rpm. Experimental data show that the rotor power output reaches its maximum at the wind speed of about 13 m/s. For wind speeds greater than 13 m/s, power decreased. WIND-II predicted a cut-out wind speed for this case at 26 m/s. Unlike theoretical predictions, the power output of the NACA 64_3-614 rotor remains nearly constant at positive power for wind speed from 25 to 29 m/s. Due to the overspeed limitation on the wind tunnel motor-dynamometer system, maximum wind speed of the tests was restricted to 29 m/s. Although tunnel velocity was limited to only 24 m/s for the rotor at 3000 rpm, similar results were obtained as shown in Figure 8(b).

In summary, the WIND-II predictions for the NACA 64_3-621 rotor, based on airfoil section data, are reasonable for low angles of attack, but poor for high angles of attack (high wind speed). The present test data are characterized by a distinct peak in the power versus wind speed plot, followed by a region of decreasing power, and then a region in which power is relatively constant with wind speed. In fact, for the case of 2000 rpm, the measured power at high wind speed exceeds the WIND-II prediction. Rasmussen (ref. 11) reported results similar to the present tests, with power initially decreasing beyond peak power, followed by constant or increasing power as wind speed is further increased. He describes "adjustments" to be made to the airfoil section data to match measured power for the high wind speed conditions. NASA Lewis Research Center test results (ref. 12) from a large-scale MOD-0A wind turbine show that the power also exceeded WIND-II predictions at high wind speeds. For the MOD-0A rotor, the power reached a maximum, and then remained constant

for higher wind speeds. The trends from the present wind tunnel tests of the NACA 64_3-621 rotor are quite similar to the Rasmussen results, and somewhat similar to the NASA MOD-0A results.

Performance Comparison Between the Two Rotor Models

Figures 9 and 10 compare the test results between the 23024 rotor and the 64_3-621 rotor. Table 2 summarizes some of the performance characteristics for both rotors. The maximum C_p for the NACA 64_3-614 rotor is nearly the same as that of the NACA 23024 rotor, but it occurs at a lower TSR. As shown in figure 9(b), the 64_3-621 rotor produces higher C_p for TSR less than about 5 but lower C_p for TSR greater than about 5. This means that at lower wind speed, the 23024 rotor produces greater power, and at high wind, the 64_3-621 rotor produces greater power. For the three rpm settings tested, the 64_3-621 rotor produces higher maximum power than the 23024 rotor (fig. 10).

Effects of Transition Strips on the Two Rotors

The purpose for this test series was to evaluate the effects of transition strips on rotor performance. The transition strips were commercial drafting chart tape. This tape is readily available and easy to apply consistently. The tape strips were attached along the entire span at 5 percent chord on the upper surface and at 10 percent chord on the lower surface of the rotor. Tests were conducted on both rotors with 0, 1, 2 and 3 transition strips (thicknesses 0.0", 0.005", 0.010" and 0.015"). The tape thicknesses are large relative to rotor thickness, but are dictated by the low Reynolds number of the tests. The Reynolds number at the tip for these test conditions is 0.3×10^6.

Figure 11 presents the results of testing the NACA 23024 rotor with 0, 1, 2 and 3 transition strips. It is shown in these figures that transition strips result in small reductions in thrust coefficient but

large penalities in power coefficient. With three transition strips installed, the NACA 23024 rotor produced negative power for all tip-speed ratios. As shown in figure 11(c), the WIND-II program accurately predicts the degradation in power coefficient for one and two trip strips, but underpredicts the power loss caused by the third trip strip.

The results of testing the transition strips on the NACA 64_3-621 rotor are shown in figure 12. For this rotor, transition strips cause a small reduction in thrust coefficient (fig. 12(a)) and also relatively small changes in power coefficient (fig. 12(b)). As shown in figure 12(c), the WIND-II program correctly predicted a small effect of transition strips on the power coefficient of this airfoil and again underpredicted the power loss from the third transition strip.

With three transition strips installed, rotor peak power is reduced from 0.21 kW to about 0.15 kW as shown in figure 12(d). With 1 or 2 transition strips installed, however, rotor peak power is increased from 0.21 kW to about 0.23 kW. The probable reason for this unexpected behavior is that the NACA 64_3-621 rotor had laminar separation on the upper surface for the low Reynolds number tested, and a trip consisting of 1 or 2 transition strips helped prevent this separation. Similar trends were reported by Rasmussen (ref. 11) who showed that transition strips penalized peak power at high rpm (high Reynolds number), but increased peak power at low rpm (low Reynolds number). His tests were on a twisted rotor with NACA 63-212/24 airfoil sections.

The most significant findings from this series of tests is that transition strips have a much larger penalty on the NACA 23024 rotor than on the NACA 64_3-631 rotor. That is, the NACA 23024 airfoil is much more sensitive to roughness than the NACA 64_3-621 airfoil. Similar trends were obtained from 2-D tests of the 23024 airfoil and the 64_3-618 airfoil at Reynolds number of 0.6×10^6, documented in WSU Report WER-16 (ref. 13).

Flow Visualization

A series of flow visualizations were conducted on the clean NACA 23024 rotor and the NACA 64_3-621 rotor. Surface flow patterns were observed using fluorescent mini-tufts attached to the upper surface (suction side) from 30 to 90 percent rotor radius at 10 percent increments along the blade span, with illumination provided by an ultra-violet strobe light. The tests were conducted at 800 rpm, with tunnel dynamic pressure varied from 0 psf (infinite TSR) to 5 psf (TSR about 1).

The purpose of these tests, as stated earlier, was to determine the extent of spanwise flow along the blade. It is believed that at angles of attack near stall, spanwise flow helps delay separation on the upper surface of the rotor, resulting in power prediction discrepancies discussed in preceding sections.

Figure 13 shows typical results of the flow visualization tests. Figure 13(a) shows the picture of the clean NACA 64_3621 rotor at infinite tip-speed ratio (0 psf tunnel dynamic pressure). The patterns of the tufts indicate only chordwise flow for all stations along the blade surface. This tuft orientation indicates that the tuft g-load or centrifugal acceleration does not have a major effect on the tufts. When the tip-speed ratio was decreased by increasing the tunnel wind velocity, spanwise flow began to develop, starting from the inboard stations. This was shown by the increasing number of tufts which turned from their original chordwise positions to point radially outward.

Table 3 summarizes the results for this series of flow visualization tests. If spanwise flow is evidence of blade stalling, the trend of the 64_3-621 rotor to encounter spanwise flow at lower TSR than the 23024 rotor seems inconsistent with the power measurements which show more positive power for the 64_3-621 rotor. Careful study of airfoil section data for the two airfoils reveals that while the 64_3-621 airfoil has a

lower initial stalling angle, the stall progression is quite slow, and the C_L curve is quite flat near the peak. Thus, this airfoil has the ability to retain high lift even when substantial separation is present.

Tests of the NACA 23024 Rotor with 30 Percent Chord Aileron

Figures 14 and 15 present the results of testing the NACA 23024 rotor equipped with a vented aileron/deflector locked in the 90^{o} degree upward position.

Figure 14 shows the comparison between the theoretical predictions from WIND-II and the experimental measurements for the gap-open aileron configuration. WIND-II predicts approximately 10 percent lower thrust coefficients for nearly all tip-speed ratios greater than 2 as shown in figure 14(a). Figure 14(b) shows a plot of power coefficient as a function of tip-speed ratio. Calculations from WIND-II show almost exactly the same results as those of the experimental measurements.

It is shown in figure 15(a) that by leaving the gap between the airfoil and the aileron open, the thrust coefficient is somewhat lower than that of the basic NACA 23024 rotor for TSR from 4 to about 8. When the gap is closed, thrust coefficients become higher than those of the basic rotor and the gap-open aileron configurations, for TSR from 1 to about 5. At this range of TSR (at high tip angles of attack), the gap-closed aileron configuration has larger profile drag area than the basic rotor and the gap-open aileron rotor configurations. At TSR greater than 5 (at low tip angles of attack), however, thrust coefficients become lower due to the loss of lift caused by the upward deflection of the aileron.

Figure 15(b) shows the effects of the aileron on the power coefficient, as a function of TSR. Both gap-open and gap-closed ailerons produced negative torque for all TSRs. Due to test limitations, the

lowest achievable TSR for the gap-open configuration was 0.65 and a TSR of 0.54 for the gap-closed configuration. The gap-open aileron configuration produced somewhat larger negative torque coefficients than the gap-closed configuration for all TSRs tested (up to about 8).

In order to determine the state of zero-torque for this model, the rotor was windmilled; that is, the rotor was driven only by the tunnel wind velocity, for a series of tunnel dynamic pressures. The TSR for the zero-torque state for the gap-open configuration was found to be -0.6, and -0.7 for the gap-closed configuration. A negative TSR means that the rotor was turning backward.

In addition, a coast-down test was conducted for the gap-open aileron configuration. For the test, the tunnel dynamic pressure was kept at 9 psf, and the rotor speed was driven to 3000 rpm, which corresponds to a tip-speed ration of about 5. The electrical power driving the rotor was then disconnected, and the rotor blade was allowed to coast down to an equilibrium zero-torque state. It took approximately five seconds for the rotor to decelerate from 3000 rpm to zero rpm and about 2 more seconds to reach the reverse-rotation equilibrium state of zero-torque at the tip-speed ratio of -0.6. Thus these tests have clearly demonstrated the ability of this configuration to protect against rotor overspeed.

The fact that the aileron-controlled rotor results in reverse rotation is not an insurmountable problem. Three solutions are possible:

(1) Allow the slow reverse auto-rotation. This rate is so low that it probably would not result in damage, even in hurricane winds.

(2) Limit aileron deflection angle to less than 90 degrees.

(3) Reduce the size of the aileron chord or lower surface extension plate.

It is recommended that an aileron of this type be tested at smaller angles of deflection (60^{o}, 70^{o} or 80^{o}) or with smaller extension plates (5, 10 or 15 percent chord) on the lower surface.

CONCLUSIONS

1. The NACA 64_3-621 rotor produces higher peak power than the NACA 23024 rotor for a given rotor speed. The NACA 23024, however, gives more power than the NACA 64_3-621 at low wind speeds.

2. Transition strip studies show that the NACA 23024 rotor is very sensitive to roughness and that when transition strips are installed, it suffers a greater penalty than the NACA 64_3-621 rotor.

3. Surface tuft studies indicate the existence of spanwise flow for a TSR less than or equal to about 1 for the NACA 23024 rotor and less than or equal about 3 for the NACA 64_3-621 rotor.

4. Analytical studies from WIND-II consistently overpredicted maximum power for the two clean rotor configurations. The predictions, however, show very good correlation with test results for operation at low wind speeds (high TSR).

5. For the purpose of loss-of-load control, the aileron configuration tested for this project is capable of producing more than enough negative torque to prevent overspeed. The unloaded rotor with aileron will rotate backward at a tip-speed ratio of -0.6.

RECOMMENDATIONS

1. Tests should be conducted to obtain low Reynolds number airfoil data for these blade sections, and these data should be used to check the analytical model.

2. The vented aileron/deflector configuration tested in this project should be evaluated on a full-scale wind turbine machine where much higher Reynolds numbers exist.

3. The aileron of this type should be tested at smaller angles of deflection (70^{o} and 80^{o}) or with smaller extension plates (5, 10 and 15 percent chord) on the lower surface to reduce negative rotation rate.

REFERENCES

1. Wentz, W. H.; Snyder, M. H.; and Calhoun, J. T.: "Feasibility Study of Aileron and Spoiler Control Systems for Large Horizontal Axis Wind Turbines," NASA CR-159856, DOE/NASA/3277-1, WER-10, NASA Lewis Research Center, 1980.

2. Wentz, W. H.; Snyder, M. H.; and Cao, H. V.: "Effects of Spoiler Hingeline Location on the NACA 23024 Airfoil," (Unpublished Interim Report) WER-27, Wind Energy Laboratory, Wichita State University, 1984.

3. Trainer, A. G.: "Overspeed Control of Horizontal Axis Wind Turbines Using Spoilers," M. S. Thesis, Wichita State University, 1984.

4. Snyder, M. H.; Wentz, W. H.; and Cao, H. V.: "Additional Reflection Plane Tests of Control Devices on an NACA 23024 Airfoil," (Unpublished Interim Report) WER-26, Center for Energy Studies, Wichita State University, 1985.

5. Snyder, M. H., and Staples, D. L.: "WIND-II Users Manual," (Unpublished Interim Report) WER-15, Wind Energy Laboratory, Wichita State University, 1982.

6. Cao, H. V.: "Performance and Aerodynamic Braking of a Horizontal-Axis Wind Turbine from Small-Scale Wind Tunnel Tests," Master of Science Thesis, Wichita State University, 1985.

7. Pope, A., and Harper, J. J.: Low Speed Wind Tunnel Testing, John Wiley and Sons, Inc., New York, 1966.

8. Abbott, I. H., and Van Doenhoff, A. E.: Theory of Wing Sections, Dover Publications, 1958.

9. Staples, D. L., and Wentz, W. H.: "Analytical Studies of Aerodynamic Braking and Control of the Mod-0 Wind Turbine with a 38 Percent Chord Vented Aileron on an NACA 64_3-621 Tip Section," (Unpublished Interim Report) PIP-13, Wichita State University, 1985.

10. Wentz, W. H.; Ostowari, C.; Manor, D.; and Snyder, M. H.: "Horizontal Axis Wind Turbine Wake and Blade Flow Measurements from Model Tests," (Unpublished Interim Report) WER-24, Wind Energy Laboratory, Wichita State University, 1984.

11. Rasmussen, F.: "Aerodynamic Performance of a New LM 17.2 m Rotor," Twelfth Meeting of Experts - Aerodynamic Calculational Methods for WECS, IEA, Copenhagen, 1984.

12. Viterna, L. A., and Janetzke, D. C.: "Theoretical and Experimental Power from a Large Horizontal-Axis Wind Turbine," NASA TM 82944, 1982.

13. Snyder, M. H.; Wentz, W. H.; and Ahmed, A.: "Two-Dimensional Tests of Four Airfoils at Angles of Attack from 0 to 360 Degrees," (Unpublished Interim Report) WER-16, Wichita State University, 1984.

APPENDIX
AIRFOIL SECTION COORDINATES

The surface contours of the airfoil tested are defined in terms of a station (distance from the leading edge) and an ordinate (distance from the chord line), expressed as a percent of the chord length.

NASA 23024 Airfoil Coordinates

Upper Surface		Lower Surface	
Station	Ordinate	Station	Ordinate
0.0	0.0	0.0	0.0
0.277	4.017	2.223	-3.303
1.331	5.764	3.669	-4.432
3.853	8.172	6.147	-5.862
6.601	9.844	8.399	-6.860
9.432	11.049	10.577	-7.647
15.001	12.528	14.999	-8.852
20.253	13.237	19.747	-9.703
25.262	13.535	24.738	-10.223
30.265	13.546	29.735	-10.454
40.256	12.928	39.744	-10.278
50.235	11.690	49.766	-9.482
60.202	10.008	59.798	-8.242
70.162	7.988	69.838	-6.664
80.116	5.687	79.884	-4.803
90.064	3.115	89.936	-2.673
95.036	1.724	94.964	-1.504
100.0	0.252	100.0	-0.252

NASA 64_3-621 Airfoil Coordinates

Upper Surface		Lower Surface	
Station	Ordinate	Station	Ordinate
-0.085	0.768	-0.085	0.768
-0.038	1.223	0.0	0.0
0.083	1.696	0.459	-0.954
0.581	2.573	1.569	-2.006
1.197	3.298	3.096	-2.851
7.045	7.260	8.455	-4.657
9.294	8.277	10.706	-5.173
15.343	10.401	13.688	-5.741
21.432	11.907	19.616	-6.577
24.486	12.475	25.514	-7.105
30.606	13.276	31.394	-7.364
39.798	13.623	40.202	-7.196
48.982	12.840	49.018	-6.223
58.124	11.296	60.841	-4.268
70.224	8.446	69.776	-2.612
79.221	5.944	78.779	-1.037
88.152	3.353	87.848	0.151
94.076	1.665	93.924	0.502
100.0	0.0	100.0	0.0

TABLE 1

Test Tip-Speed Reynolds numbers and Tip-Speed Mach numbers.

Configuration	Re_t		M_t	
	Minimum	Maximum	Minimum	Maximum
NACA 23024 Rotor	0.11×10^6	0.58×10^6	0.08	0.43
NACA 23024 Rotor with 0.30c Aileron, Gap Open	0.11×10^6	0.37×10^6	0.10	0.28
NACA 23024 Rotor with 0.30c Aileron, Gap Closed	0.11×10^6	0.38×10^6	0.10	0.28
NACA 64_3-621 Rotor	0.12×10^6	0.56×10^6	0.09	0.43

TABLE 2

Performance Comparison

Model	TSR at C_p=0	TSR at Maximum C_p	Maximum C_p
NACA 23024 Rotor	1.5,4.0, 8.0	5.18	0.318
NACA 64_3-621 Rotor	6.7	4.40	0.302

TABLE 3

Spanwise Flow Observations From Tuft Studies (@ 800 RPM).

q (lb/ft^2)	V (ft/sec)	TSR	Re_t (million)	M_t	Spanwise Flow	
					NACA 23024	NACA 64_3-621
0.0	0.0	∞	0.0839	0.0625	none	none
0.20	13.41	5.20	0.0854	0.0637	Root to 0.4-R	Root to 0.6-R
0.40	18.97	3.68	0.0869	0.0648	Root to 0.5-R	Root to 0.7-R
0.60	23.23	3.00	0.0884	0.0659	Root to 0.6-R	Root to 0.9-R
0.80	26.83	2.60	0.0899	0.0670	Root to 0.6-R	Root to Tip
1.00	29.99	2.33	0.0913	0.0681	Root to 0.7-R	↓
1.50	36.74	1.90	0.0948	0.0707	Root to 0.8-R	
2.00	42.42	1.65	0.0981	0.0732	Root to 0.8-R	
5.00	67.07	1.04	0.1154	0.0867	Root to 0.9-R	

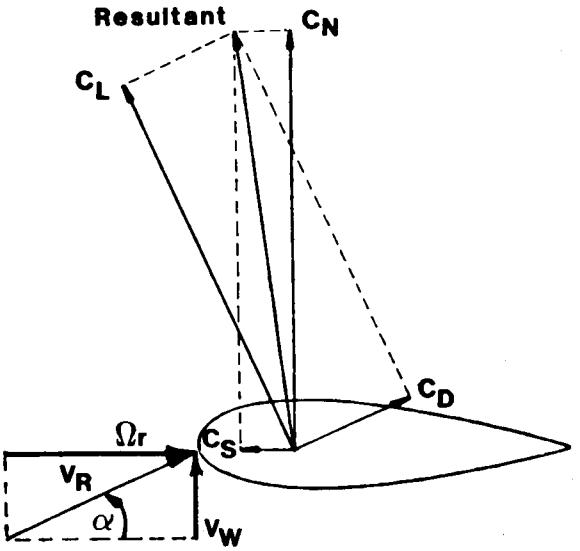

Figure 1. - Forces on a wind turbine blade element.

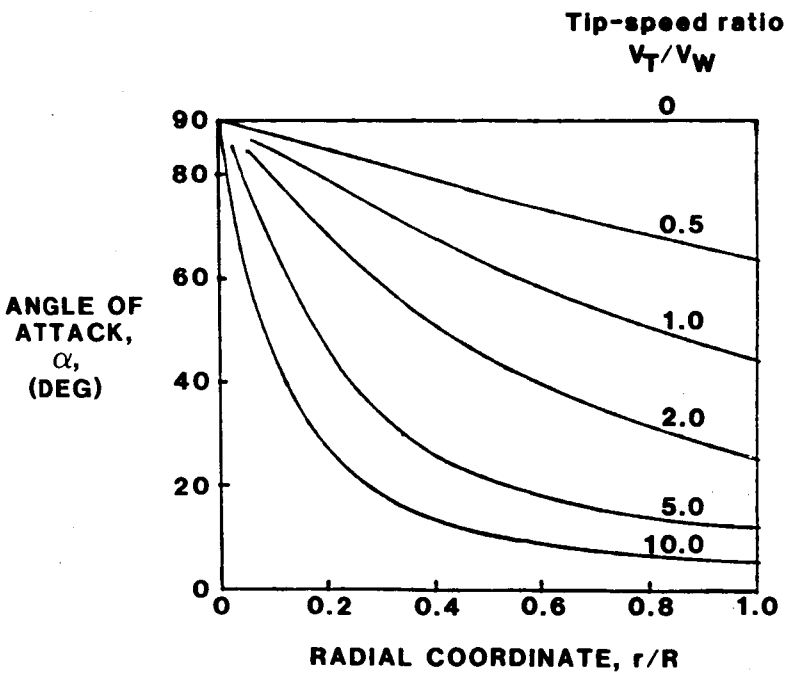

Figure 2. - Effect of tip-speed ratio on angle of attack as a function of radial position along blade.

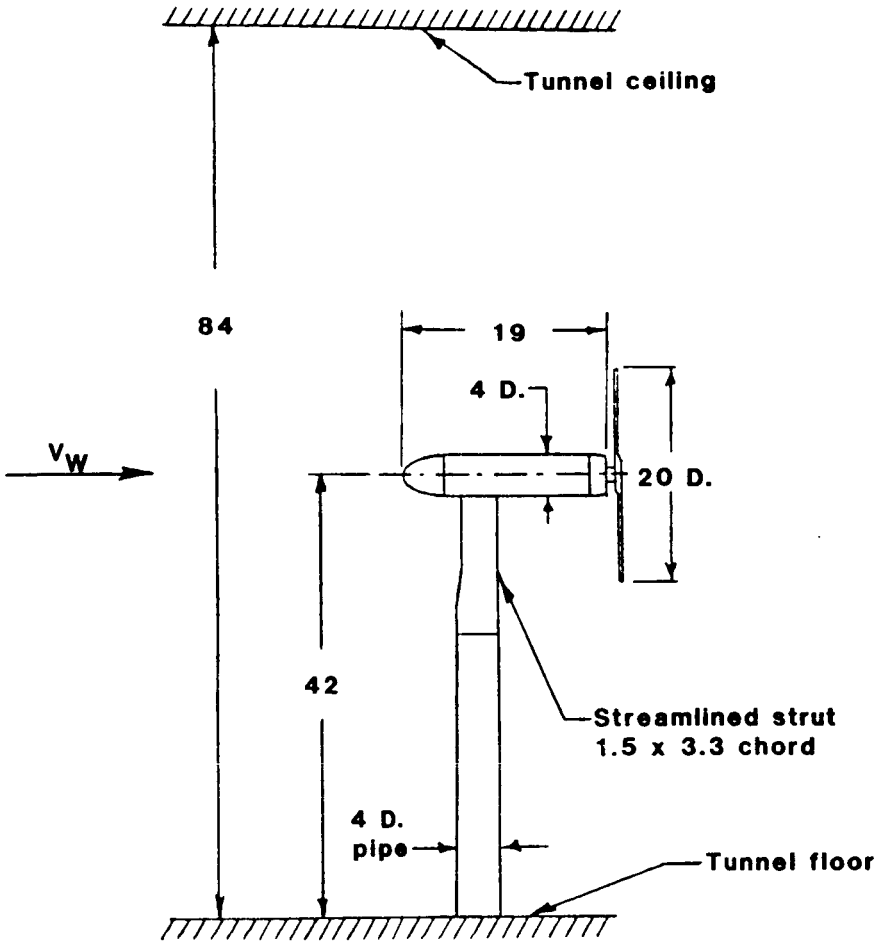

Figure 3. - Wind tunnel test section and installation of test rotor (all dimensions in inches).

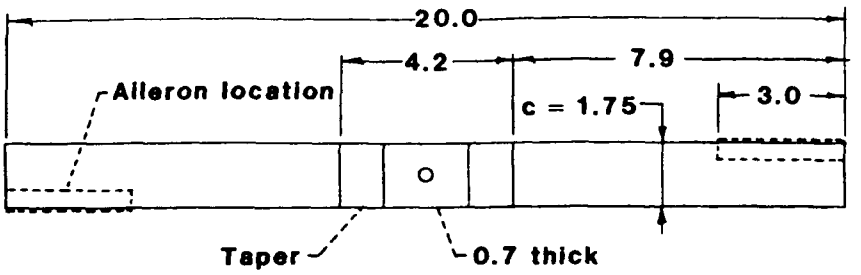

(a) Rotor planform (dimensions in inches).

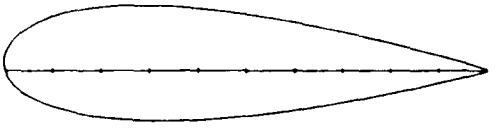

(b) NACA 23024 airfoil.

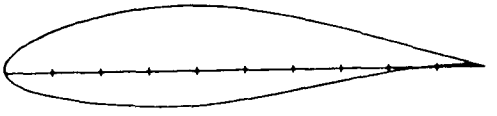

(c) NACA 64_3-621 airfoil.

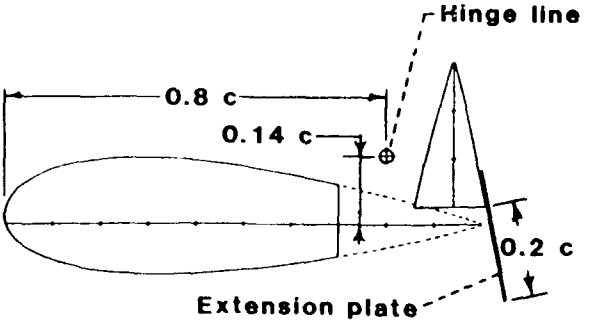

(d) NACA 23024 airfoil with aileron deflected -90^{o} and gap open.

Figure 4. - Geometry of test rotors (airfoil coordinates are given in the Appendix).

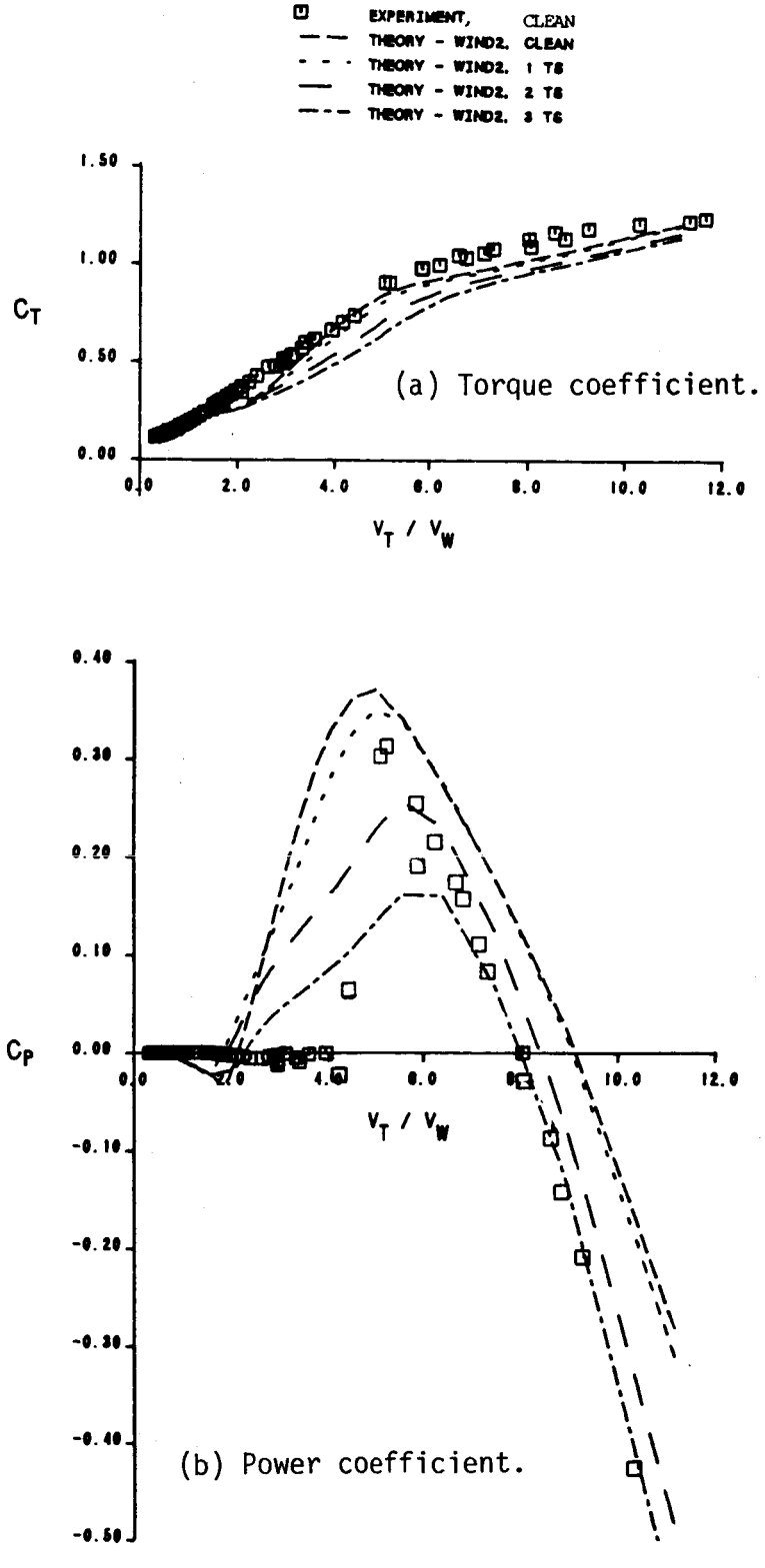

Figure 5. - Effect of TSR on performance of the NACA 23024 rotor, compared with theory.

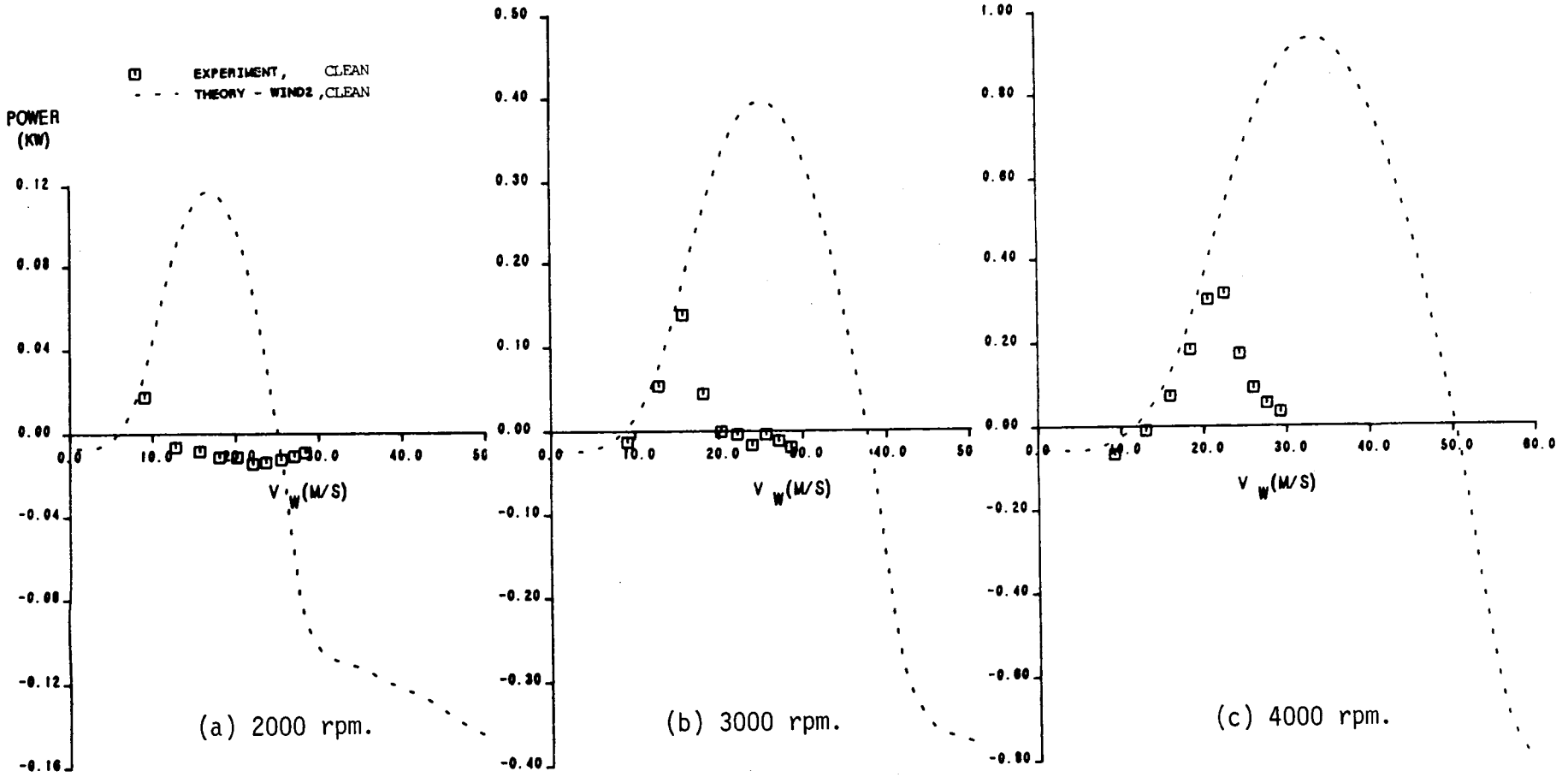

Figure 6. - Effect of wind speed on power of the NACA 23024 rotor, compared to theory.

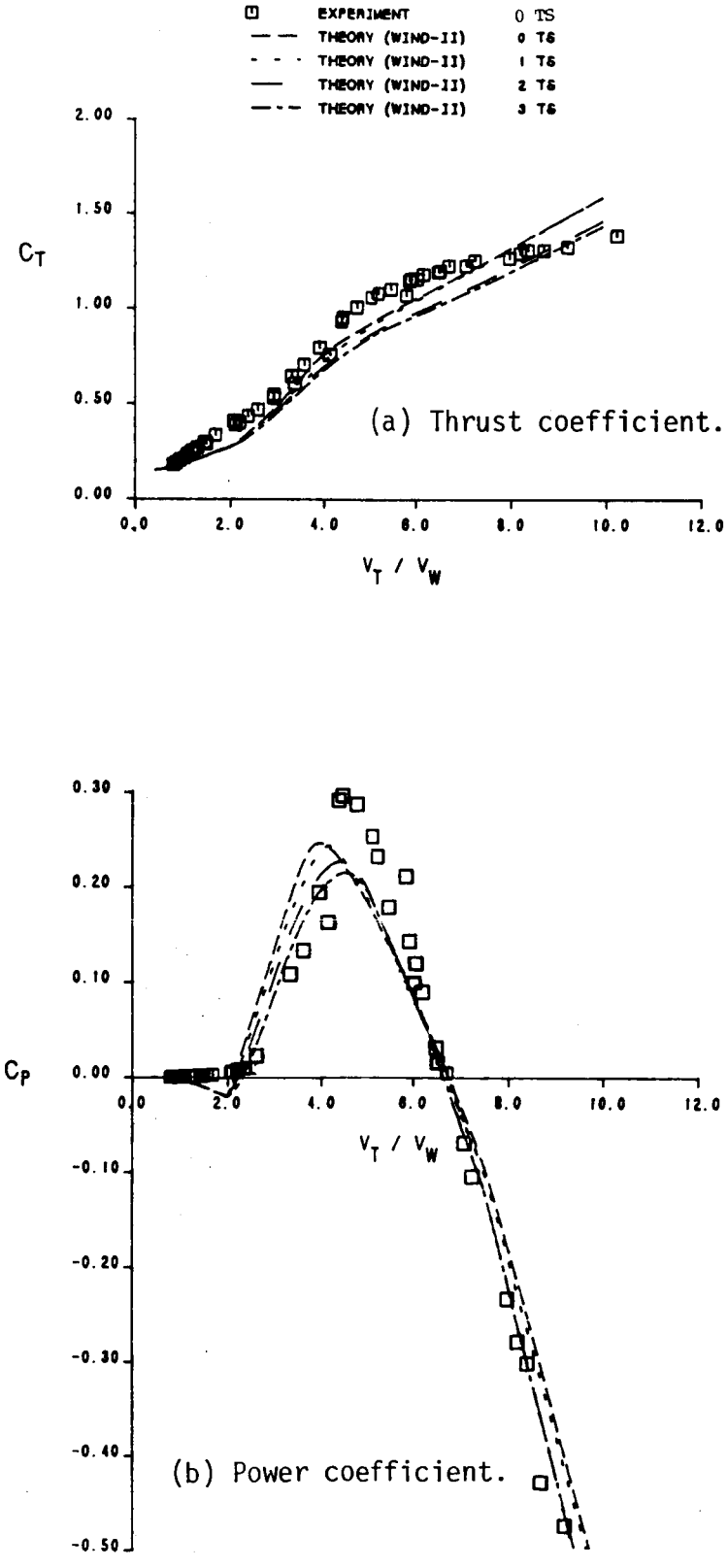

Figure 7. - Effect of TSR on performance of the NACA 64_3-621 rotor, compared with theory.

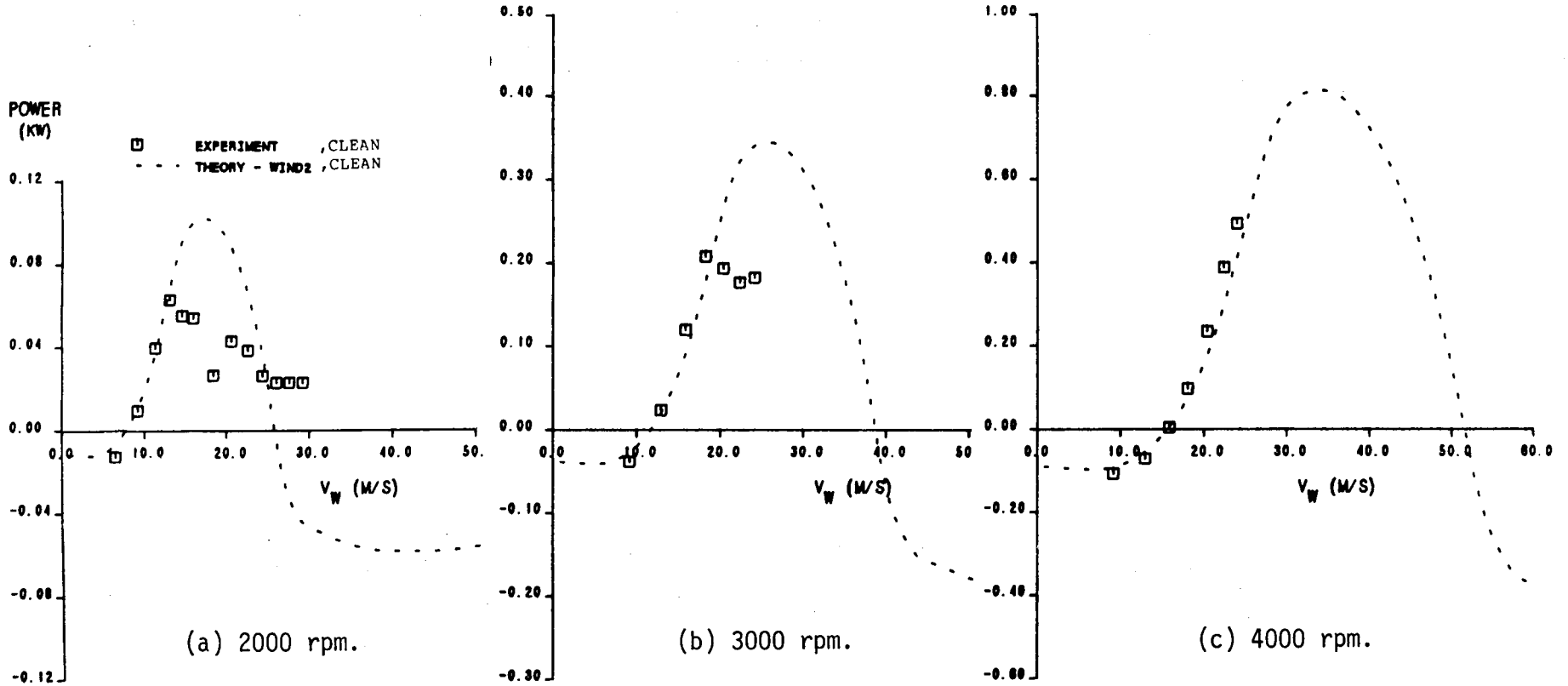

Figure 8. - Effect of wind speed on power of the NACA 64_3-621 rotor, compared to theory.

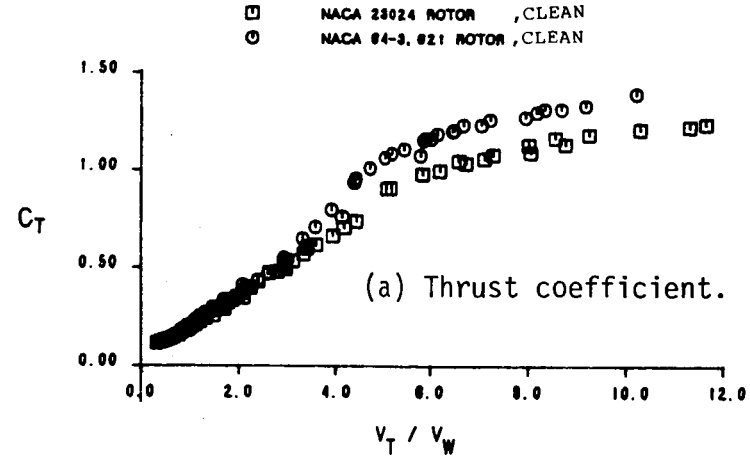

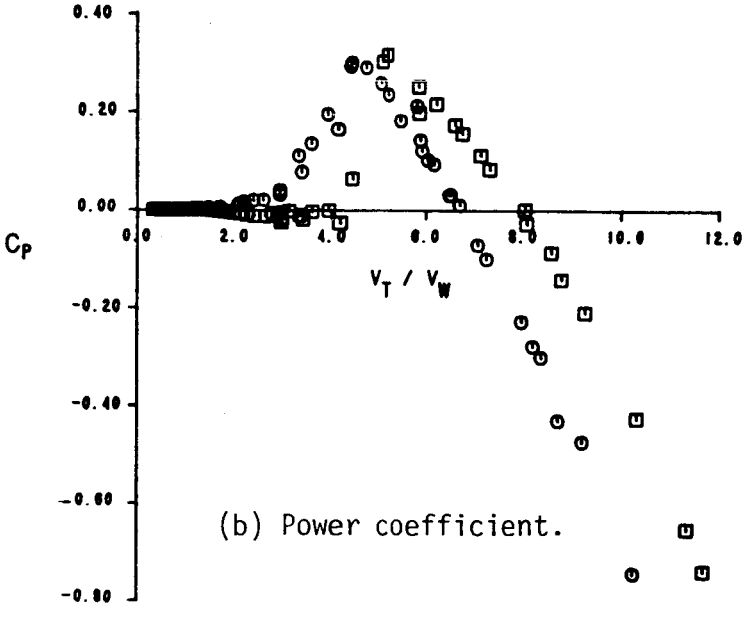

Figure 9. - Performance comparison between the NACA 23024 and NACA 64_3-621 rotors.

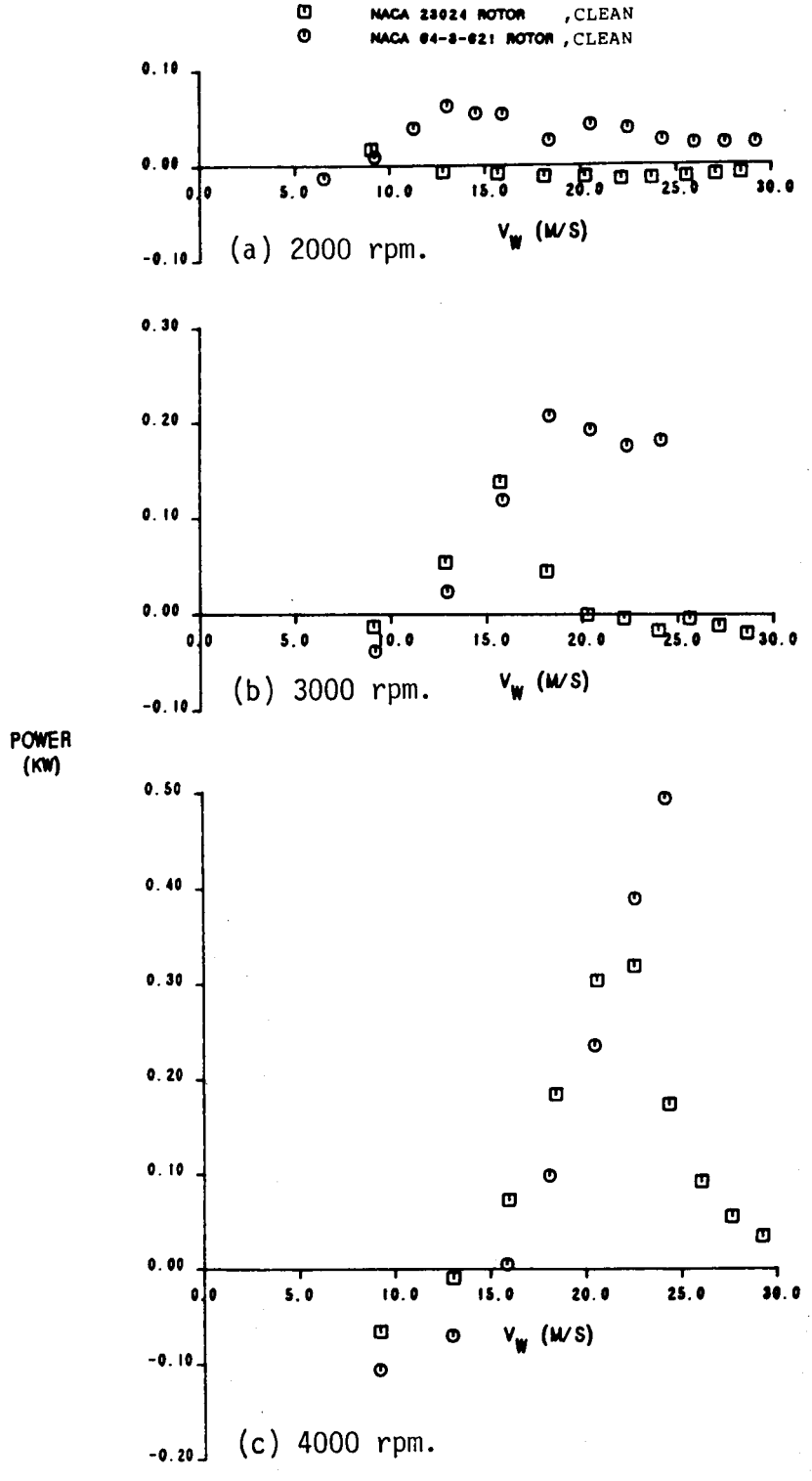

Figure 10. - Power comparison between the NACA 23024 and NACA 64_3-621 rotors.

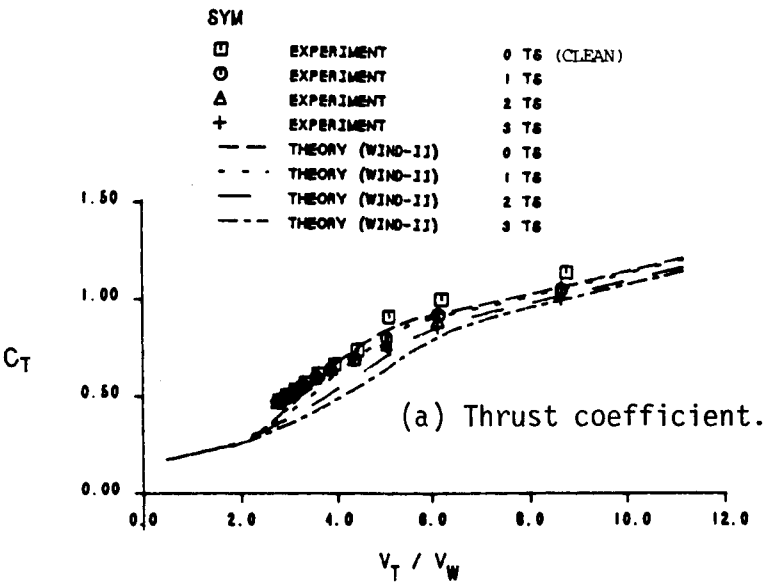

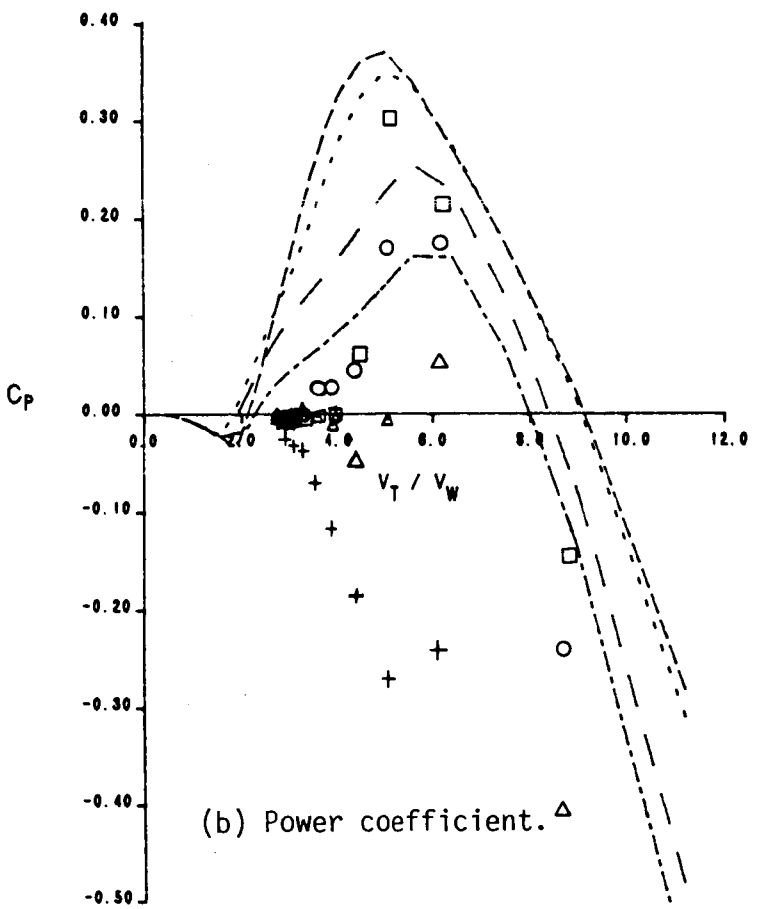

Figure 11. - Effect of transition strips on performance of the NACA 23024 rotor at 3000 rpm.

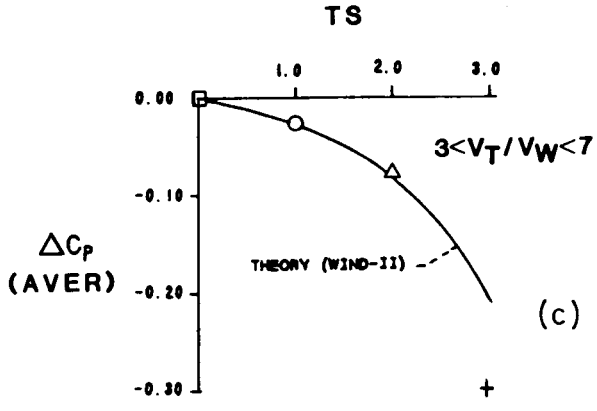

(c) Average change in power coefficient.

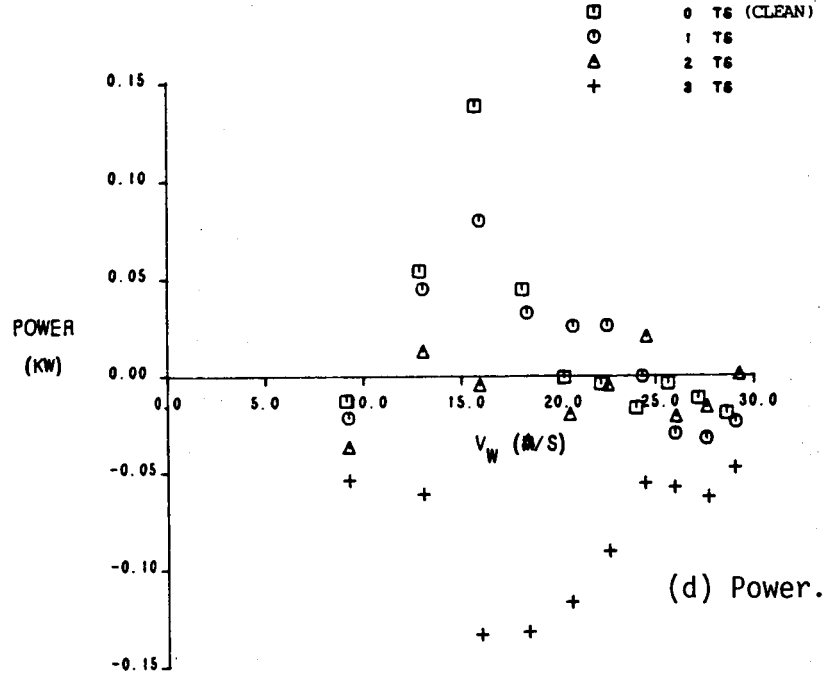

(d) Power.

Figure 11. - Concluded.

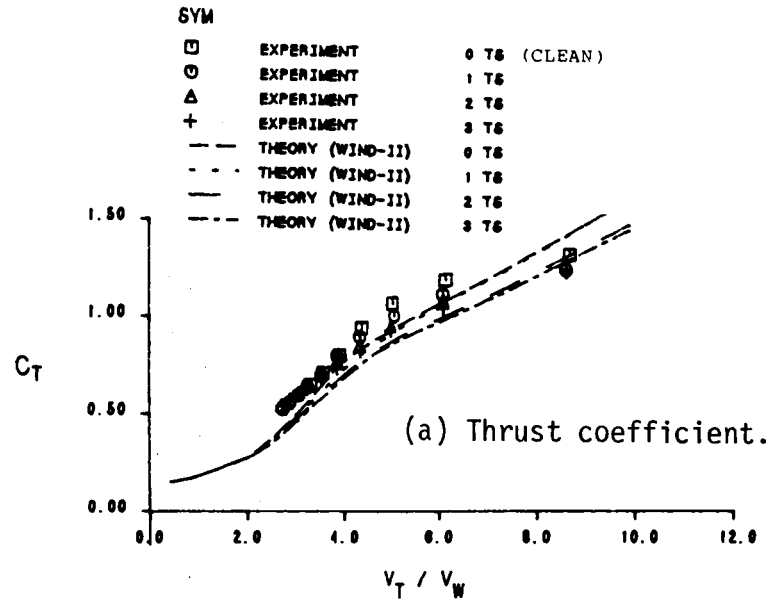

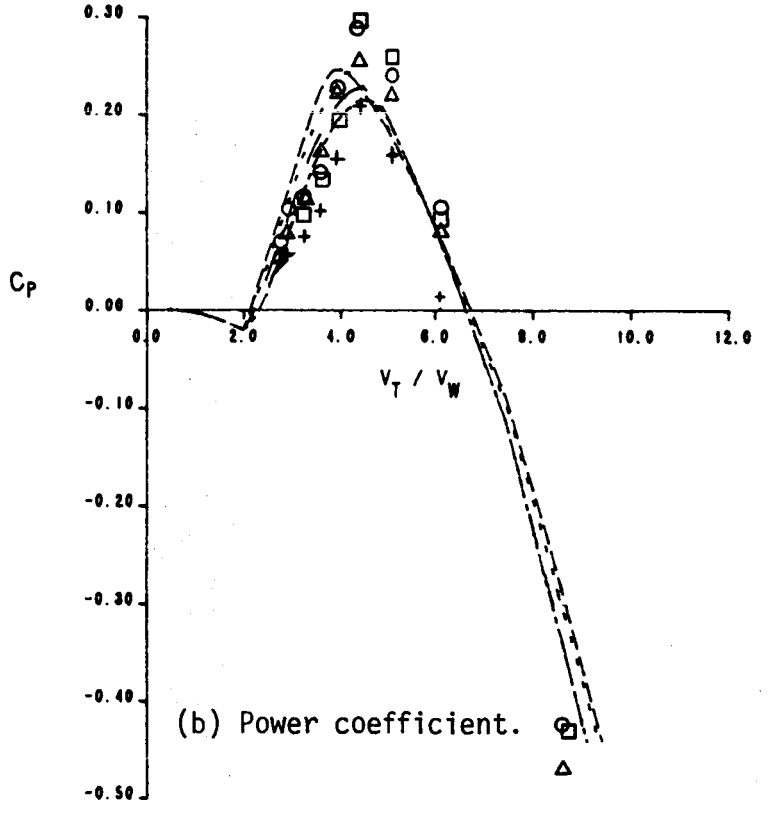

Figure 12. - Effect of transition strips on performance of the NACA 64_3-621 rotor.

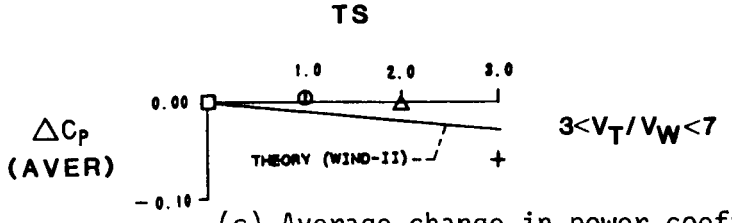

(c) Average change in power coefficient.

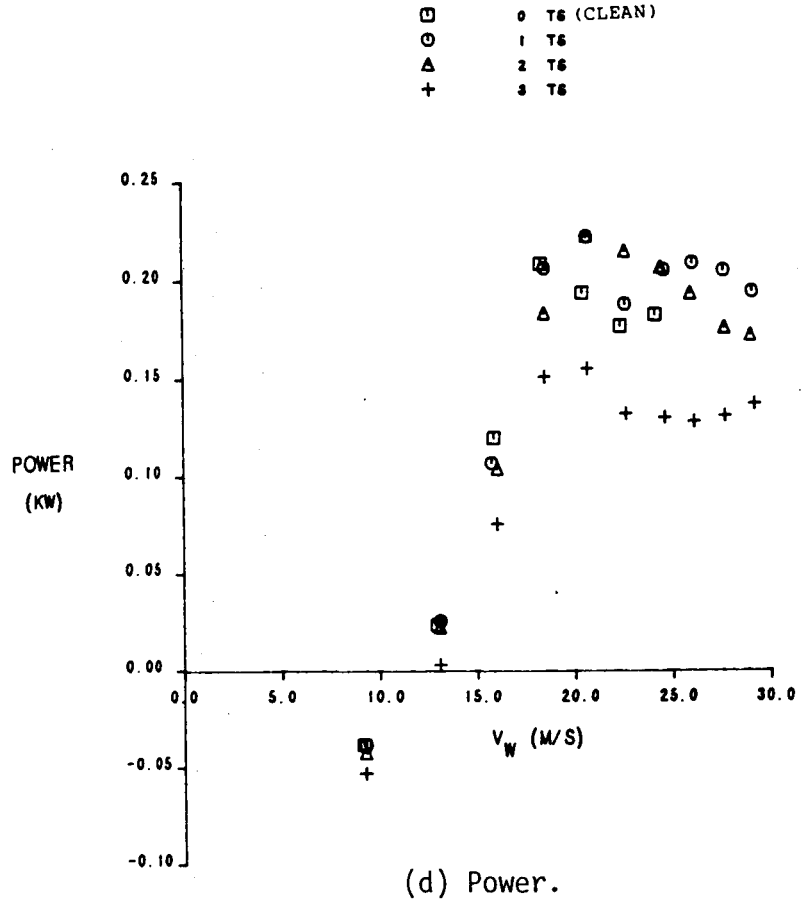

(d) Power.

Figure 12. - Concluded.

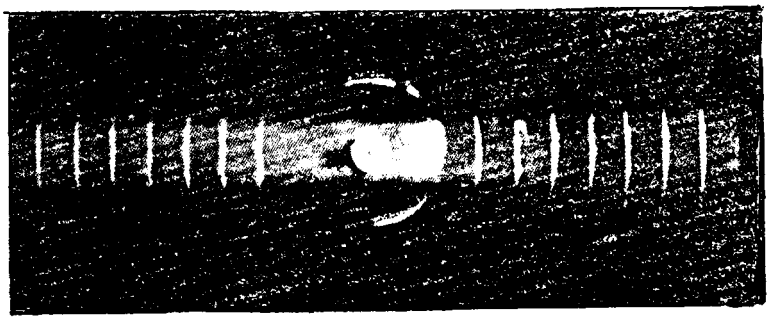

(a) At TSR = ∞ tufts are chordwise, indicating no spanwise flow along the blades.

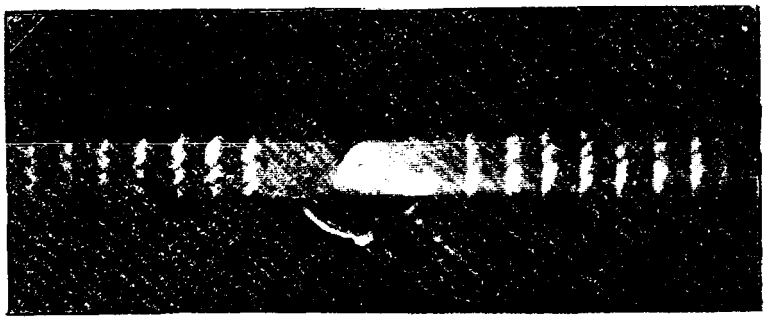

(b) At TSR = 2.33 tufts turn radially outward, indicating spanwise flow from hub to blade tips.

Figure 13. - Typical flow visualization results, from tests of the NACA 64_3-621 rotor at 800 rpm (clockwise rotation).

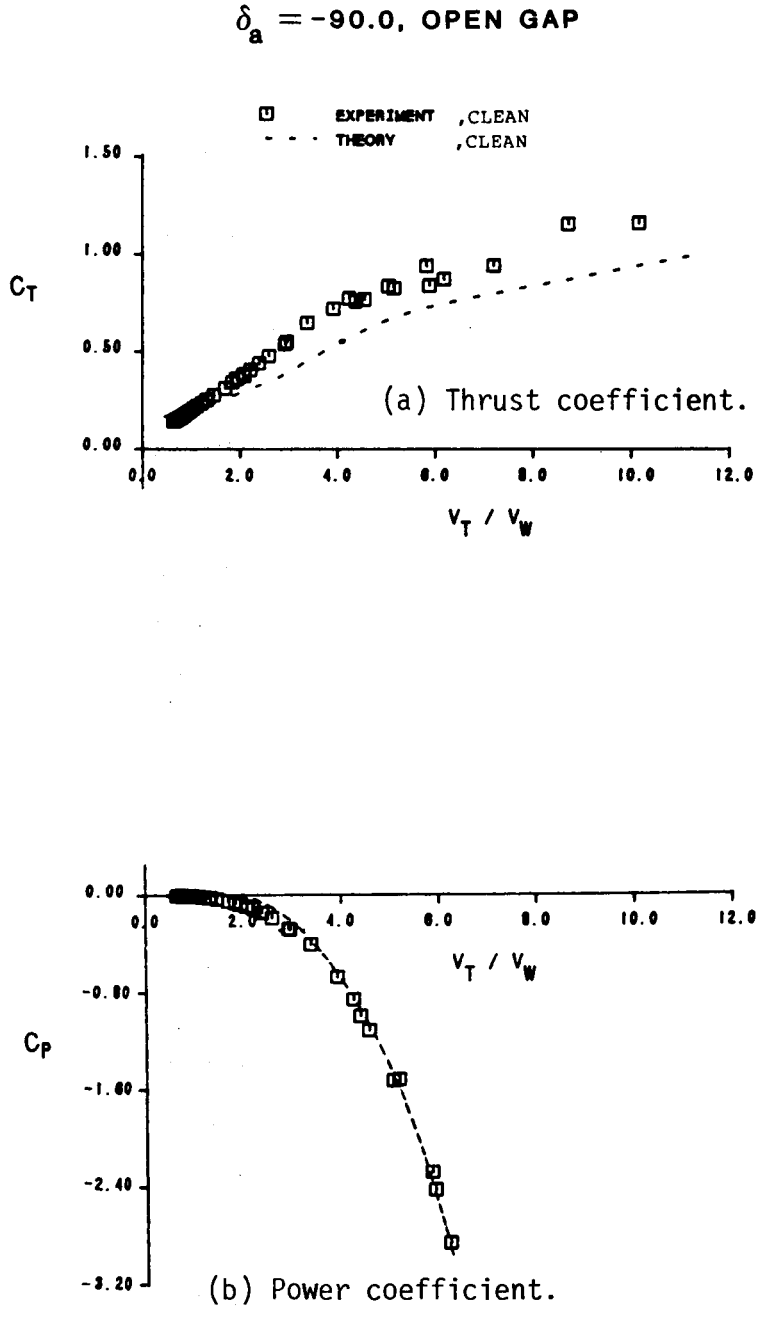

Figure 14. - Effect of TSR on performance of the NACA 23024 rotor with a 30%-chord aileron fully deflected and the gap open, compared with theory.

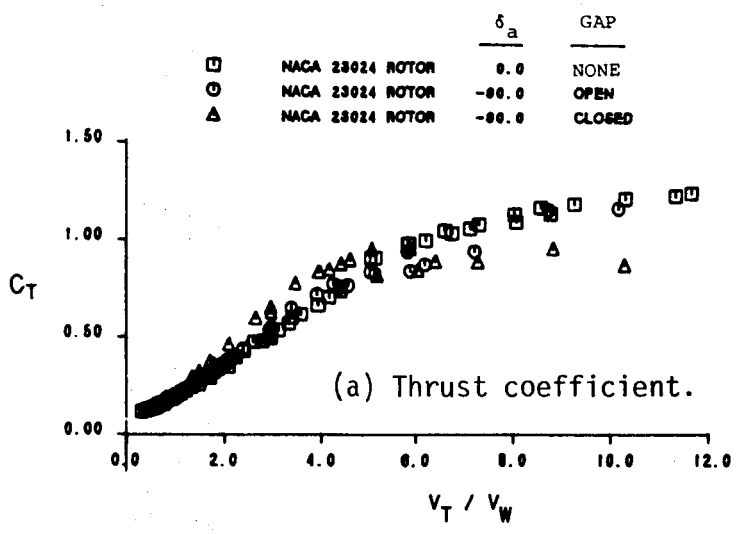

(a) Thrust coefficient.

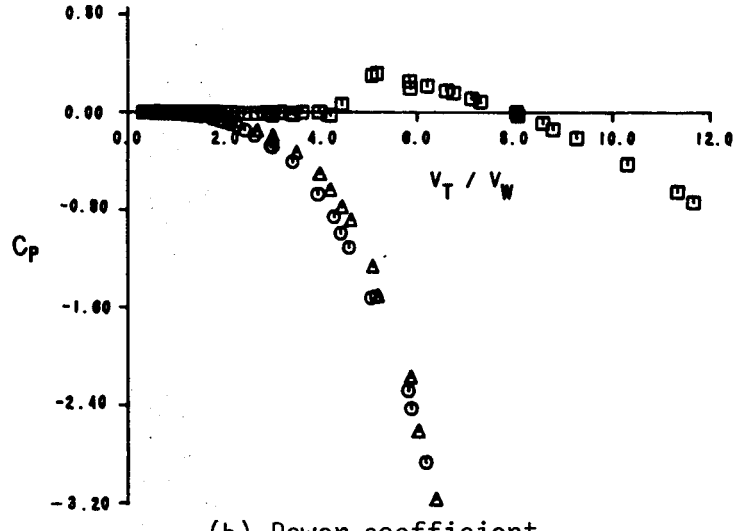

(b) Power coefficient.

Figure 15. - Effect of aileron deflection, gap position, and TSR on performance of the NACA 23024 rotor with a 30%-chord aileron.

NASA
National Aeronautics and Space Administration

Report Documentation Page

1. Report No.	2. Government Accession No.	3. Recipient's Catalog No.
NASA CR-180812		

4. Title and Subtitle	5. Report Date
Performance and Aerodynamic Braking of a Horizontal-Axis Wind Turbine from Small-Scale Wind Tunnel Tests	July 1987
	6. Performing Organization Code

7. Author(s)	8. Performing Organization Report No.
H.V. Cao and W.H. Wentz, Jr.	
	10. Work Unit No.

9. Performing Organization Name and Address	11. Contract or Grant No.
Wichita State University Wichita Falls, Kansas 67208	NSG-3277
	13. Type of Report and Period Covered
12. Sponsoring Agency Name and Address	Contractor Report
U. S. Department of Energy Wind/Ocean Technology Division Washington, D. C. 20545	14. Sponsoring Agency Report No. DOE/NASA/3277-4

15. Supplementary Notes

Final Report. Prepared under Interagency Agreement DE-AI01-76ET20320. Project Manager, J.M. Savino, Structures Division, NASA Lewis Research Center, Cleveland, Ohio 44135.

16. Abstract

Wind tunnel tests of three 20-inch diameter, zero-twist, zero-pitch wind turbine rotor models have been conducted in the WSU 7' x 10' wind tunnel to determine the performance of such rotors with NACA 23024 and NACA 64_3-621 airfoil sections. Aerodynamic braking characteristics of a 38 percent span, 30 percent chord, vented aileron configuration were measured on the NACA 23024 rotor. Surface flow patterns were observed using fluorescent mini-tufts attached to the suction side of the rotor blades. Experimental results with and without ailerons are compared to predictions using airfoil section data and a momentum performance code. Results of the performance studies show that the 64_3-621 rotor produces higher peak power than the 23024 rotor for a given rotor speed. Analytical studies, however, indicate that the 23024 should produce higher power. Transition strip experiments show that the 23024 rotor is much more sensitive to roughness than the 64_3-621 rotor. These trends agree with analytical predictions. Results of the aileron tests show that this aileron, when deflected, produces a braking torque at all tip-speed ratios. In free-wheeling coastdowns the rotor blade stopped, then rotated backward at a tip-speed ratio of -0.6. Results of the tuft studies indicate that substantial spanwise flow develops as blade stall occurs at low tip-speed ratios.

17. Key Words (Suggested by Author(s))	18. Distribution Statement
Wind energy; Wind turbine; Aerodynamic performance; Aerodynamic braking; Flow visualization; Aileron braking; Wind tunnel test; Model rotor test; Wind turbine model	Unclassified - unlimited Subject Category 44 DOE Category UC-60

19. Security Classif. (of this report)	20. Security Classif. (of this page)	21. No of pages	22. Price*
Unclassified	Unclassified	40	A03

*For sale by the National Technical Information Service, Springfield, Virginia 22161